General Research Profile (Minor): Research Project

A mutagenesis study of the antibiotic plectasin and the implications on its mode of action against MRSA

Mick van der Weijde
5697506

Under supervision of:

Dr. Markus Weingarth – Utrecht University

And the daily supervision of:

Maik. G. N. Derks, MSc

Examiners:

Dr. Markus Weingarth – Utrecht University

Dr. Eefjan Breukink – Utrecht University

July 2022

Abstract

The threat of antimicrobial resistance (AMR) is becoming a greater threat to the world's healthcare. To combat AMR, there is a need to search and develop novel antibiotics. Plectasin is such novel antibiotic. It targets lipid II (LII), which is often referred to as the 'Achilles heel' of the cell. LII is an indispensable for the bacterium's survival. It is the major building block for the bacterial peptidoglycan network and once disturbed, leads to rapid cell death. Plectasin is a cysteine-stabilized αβ defensin and a derivative of plectasin, NZ2114, is a triple mutant that has dramatically increased activity against methicillin-resistance *Staphylococcus aureus*, one of the most dangerous drug-pathogen combinations. The three mutations (D9N, M13L, Q14R) in NZ2114 however do not overlap with the suggested LII binding site, and no rationale why these mutations increase the efficacy against MRSA could be found thus far.

Here, we investigated the effect of the three mutations on the efficacy of plectasin against MRSA, MSSA and Staphylococcus simulans using a combination of solution NMR, bacterial killing assays, and isothermal titration calorimetry (ITC) experiments. We found that mutations D9N and Q14R drastically increase plectasin's activity against MRSA. The D9N mutation causes many chemical shift perturbations (CSP), specifically in the anionic patch and β-loop region that bind Ca^{2+} and W8 and F35 which are suggested to bind the sugars of LII. Mutations M13L and Q14R do not cause CSP in the Ca^{2+} binding site, but do cause CSP in the α-helix, which is responsible for oligomerization of plectasin.

Layperson abstract

We are facing a huge threat to the worlds general healthcare due to the widespread and careless use of antibiotics. Antimicrobial resistance (AMR) occurs when microbes, such as bacteria, develop mechanisms that make antibiotics ineffective. To combat AMR, we need to search or develop novel antibiotics that are very effective against these superbugs, very difficult to develop resistance towards and that are broadly applicable towards many bacteria. However, big pharmaceutical companies are backing out due to the high cost to search and develop these drugs with very little in return. Antibiotics that meet the requirements have to have an outstanding target within the bacteria.

One such target is lipid II (LII), as it is the major building block for the bacterial cell wall and often referred to as its 'Achilles heel'. LII is essential in the bacteria's survival as it is responsible for its size and shape, its protection against the outside, its reproduction, and many other function. LII is made inside the cell membrane of the bacteria and after incorporated in the cell wall. Once the peptidoglycan network is disrupted, by for instance the sequestering of LII from being incorporated, the bacteria will rapidly die.

A novel antibiotic that targets LII and the main focus of the report is plectasin. Many studies have been performed on plectasin and it's a representative of a major class of new antibiotics. From the research, we now know that it targets two parts of LII, which are highly unlikely to be modified, in turn making plectasin a very difficult antibiotics to gain resistance towards. Plectasin has also been shown to be highly active in infected mice models with low toxicity towards the animal. NZ2114 is plectasin that has three mutations which makes it more active against one of the most dangerous superbugs: methicillin-resistant *Staphylococcus aureus* (MRSA). These three mutations do not correlate with the way plectasin would bind to LII and there was no knowledge about how these three mutation would increase plectasin's ability to kill MRSA. The three mutations in NZ2114 do correlate to the binding site that plectasin has with calcium ions. These calcium ions play a very important role in the antibacterial activity of plectasin, but how the calcium ions and the mutations influence the binding of plectasin to LII is currently unknown.

This study aimed to shed light on the effect of the three mutations in plectasin that lead to increased activity against MRSA. Here, we used did the mutagenesis to produce plectasin with one of the three or two of the three mutations. After production and purification of plectasin, we inspected the structure of all our plectasins. These six different mutants, the normal plectasin and NZ2114 were compared to each other for their effectivity in killing MRSA and their binding affinity to LII. We found one mutation causes a large change in the calcium ion binding site and maybe the LII binding site, which also increases the killing activity. The other mutants cause a change in the structure which might make NZ2114 more likely to stick to other NZ2114 molecules. This in turn helps NZ2114 in killing MRSA. Another option for the increased activity is caused by changing the overall charge of the antibiotic, from +1 to +3, due to the mutations. This may help the more positively charged NZ2114 to bind LII as it is less repelled by the very negatively charged bacterial cell membrane.

Table of contents

Introduction

Antimicrobial resistance and the need for novel antibiotics

In the recent years, it has become more and more apparent that antimicrobial resistance (AMR) is a major threat to our general health[1,2]. Due to the use and abuse of antibiotics in hospitals, but also in nonmedical use cases, bacteria are gaining more resistance to the widely used but also the last resort drugs[3]. To combat this problem, new antimicrobial drugs or alternatives have to be developed[4,5]. The discovery and development of such drugs is time intensive, the drugs might not get approved, they are very costly to develop and make and thus isn't profitable for the big pharma[6,7]. Academia can provide insights into the working mechanisms of antimicrobial drugs, which can then be used in the drug development process reducing loss and ensuring a steady stream of novel compounds.

The World Health Organisation (WHO) has on multiple occasions published a list of 'priority pathogens'[8–10], which are a major cause of disease and deaths every year for millions of people worldwide[2,11]. More recently, a study has been able to attribute 1.2 million deaths to AMR and 4.9 million cases AMR associated deaths[1]. Their findings also include the leading pathogens for deaths associated with AMR (*Escherichia coli*, *Staphylococcus aureus*, *Klebsiella pneumoniae*, *Streptococcus pneumoniae*, *Acinetobacter baumannii* and *Pseudomonas aeruginosa*) and the most prevalent pathogen-drug combination associated with AMR deaths, which was methicillin-resistant *S. aureus* (MRSA).

Lipid II as ideal antibiotic target

A strategy to combat AMR is to develop antibiotics with a target that is essential, difficult to modify and conserved in between bacterial species. One such target is lipid II (LII), often referred to as the 'Achilles heel' of bacteria[12]. LII is a crucial building block in the peptidoglycan (PGN) synthesis of bacteria. The PGN layer is present in both Gram-negative and -positive bacteria, however it is mostly present as a single layer in between the inner and outer membrane of Gram-negative bacteria and present as much larger multi-layered cell wall on the outside of Gram-positive bacteria[13]. The PGN is readily accessible in Gram-positive bacteria, which makes the biosynthesis proteins, lipid II itself and its precursors outstanding targets for antibiotics[14]. The general structure of LII consist of the undecaprenyl phosphate (C_{55}-P) that is linked via a pyrophosphate to N-acetyl-muramyl-pentapeptide-N-acetylglucosamine (MurNAc-pp-GlcNAc) disaccharide (Figure 1A)[13]. The biosynthesis is a multistep process spanning three cell compartments: the cytoplasm, the inner face of the inner membrane and the outer face of the inner membrane. After crossing over to the outer face of the membrane, the disaccharide is transferred to a nascent chain (Figure 1B).

Disruption of the LII biosynthesis leads to dysfunction of the bacteria, as the PGN is responsible for many critical functions, such as cell integrity and reproduction[15]. There are a variety of LII binders that target different components of LII[16]. The (glyco-)lipopeptide vancomycin[17] binds LII on the D-Ala-D-Ala of the pentapeptide, which can be altered by bacteria to D-Ala-D-Lactate to acquire resistance. Other LII binders target the pyrophosphate and MurNAc sugar, *i.e.* the depsipeptide teixobactin[18], the lantibiotic nisin[19] and the defensin plectasin[20]. The pyrophosphate of LII is an ideal target, as it cannot be modified.

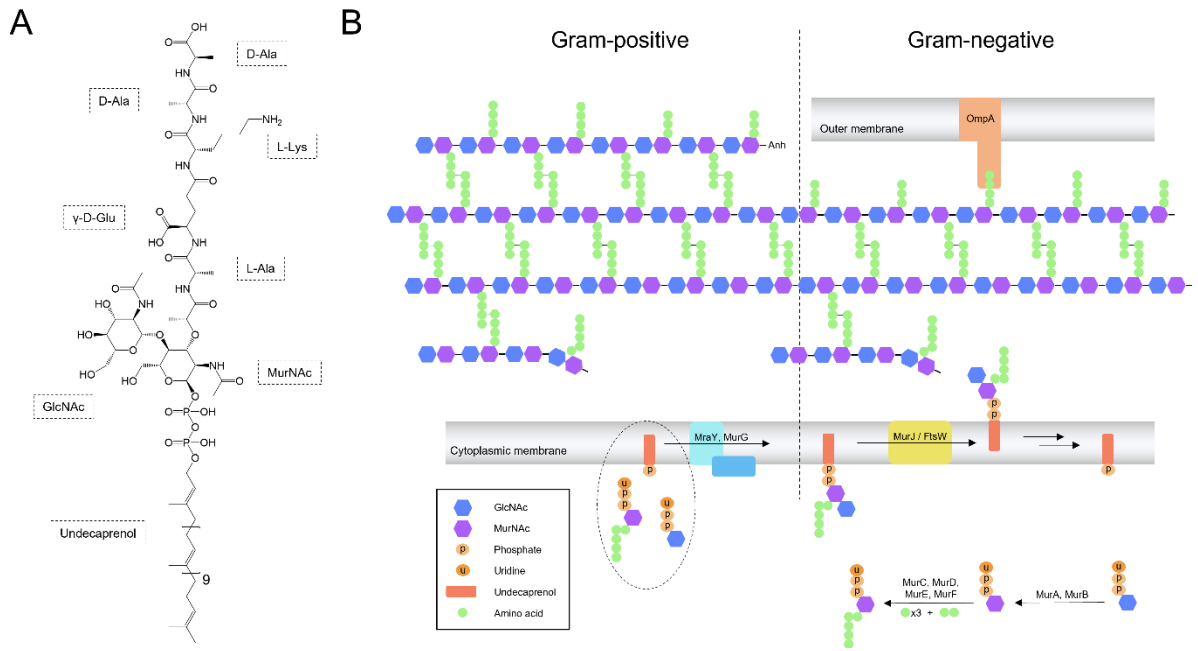

Figure 1. (A) The structure of lipid II (LII). LII consists of a undecaprenol lipid tail (C55) coupled the sugars MurNAc-GlcNAc by a pyrophosphate. On the MurNAc sugar is the pentapeptide. In this depiction it is based on LII of most Gram-positive bacteria, in which the pentapeptide consists of L-Ala-D-Glu-L-Lys-D-Ala-D-Ala. (B) A schematic depiction of the peptidoglycan (PGN) for Gram-positive and Gram-negative bacteria and a schematic overview of the biosynthesis of LII. After synthesis of LII in the cytoplasm, the LII is flipped to the outer leaflet by a flippase, where it can then be incorporated into the PGN. Most Gram-negative bacteria only contain a single layer of PGN, while Gram-positive bacteria have a multi-layered PGN.

Plectasin and plectasin-derivatives

Plectasin is a 40 residue long cysteine-stabilized αβ (CSαβ) defensin, isolated from the fungus *Pseudoplectania nigrella*[20,21]. It contains 3 disulfide bonds (C4–C30, C15–C37, C19–C39), an α-helix (M13–S21) and two antiparallel beta-strands (G28–A31, V36–C39) (Figure 2). Curiously, plectasin contains a negative patch (D9-E10-D11-D12) at the end of the first loop right before the α-helix, which is not present in other known CSαβ defensins. Recent studies show that plectasin can bind divalent cations[22,23] and this may be related to the anionic patch and antibacterial activity[23,24]. Plectasin does not only bind Ca^{2+} with the amides of the anionic patch residues (excluding D9), but also the amides of residues A31-K32-G33-G34 and the side chain of N5 and Q14[25].

Its exact mode of action however remains unidentified. The killing might occur, like many other LII binders, by sequestering the LII from incorporation into the PGN. Another common AMP mode of action is by pore formation, however literature suggest that pore formation is not its only mode of action, if it occurs at all in biological membranes[26,27]. Plectasin's minimal inhibitory concentration (MIC) and minimal bactericidal concentration (MBC) are very close together[20,21], suggesting it kills the bacteria and not only halting its replication. We can also observe oligomerisation of the LII-plectasin complex, like other LII-targeting antibiotics[18], using ssNMR DNP experiments[25], high speed AFM studies and fluorescent microscopy (unpublished data).

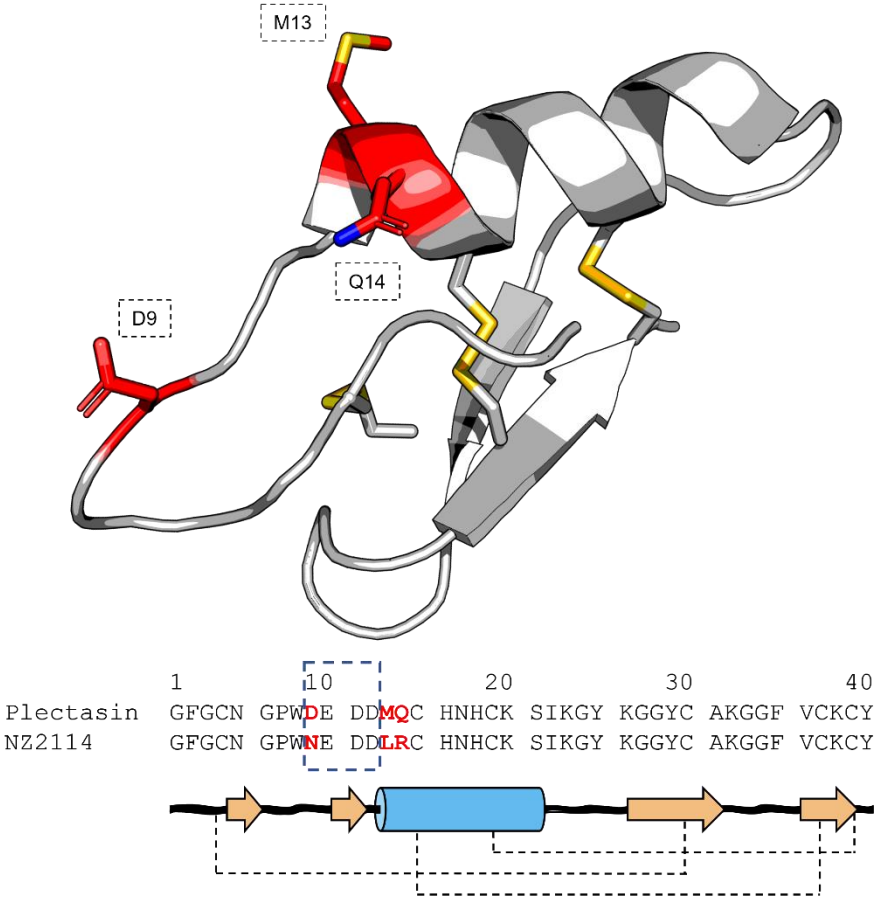

Figure 2. Schematic view of wildtype plectasin. Residues 9, 13 and 14 (indicated in red) will be studied in this research by way of mutagenesis, NMR, ITC and inhibitory studies. We will focus on mutations D9N, M13L and Q14R, single and double mutants, as these three mutations together improve plectasin MIC against MRSA. NZ2114, as the triple mutant is called, has been described to have a similar fold as wildtype plectasin. Residues D9-E10-D11-D12 are commonly referred to as the anionic or negative patch and is the binding site for Ca^{2+}.

Some natural and synthetic derivatives include NZ2114 (D9N, M13L, Q14R)[28,29], MP1102 (D9, M13, Q14)[30] and Py4 (Q14K, G33A)[31]. These examples all contain a mutation on Q14 and to a lesser extent D9 and M13, and all have increased activity against MRSA. In this research we will be taking a closer look at NZ2114. This triple mutant has a +3 net charge (to plectasin's +1) and the mutations do not correlate to the LII binding site, however they are very close to (M13, Q14) or are part of the negative patch (D9). Interestingly, these three mutations increase the activity against MRSA, while the overall fold is still conserved[23,25,32,33]. LII of MRSA has two distinct structural changes: the E2 of the pentapeptide is amidated and the K3 contains a pentaglycine chain[34,35]
In this study, we aim to better understand the influence of the three point mutations in plectasin, D9N, M13L, and Q14R that lead to an increase in anti-MRSA activity. We will discuss in short the production and purification of plectasin and the mutants (Figure 3), which consist of site-directed mutagenesis and purification via Ni^{2+} affinity and gel-filtration chromatography. The main results were produced by solution NH NMR, MIC studies and ITC to observe the increase in anti-MRSA activity and LII binding between the mutants compared to the wildtype.

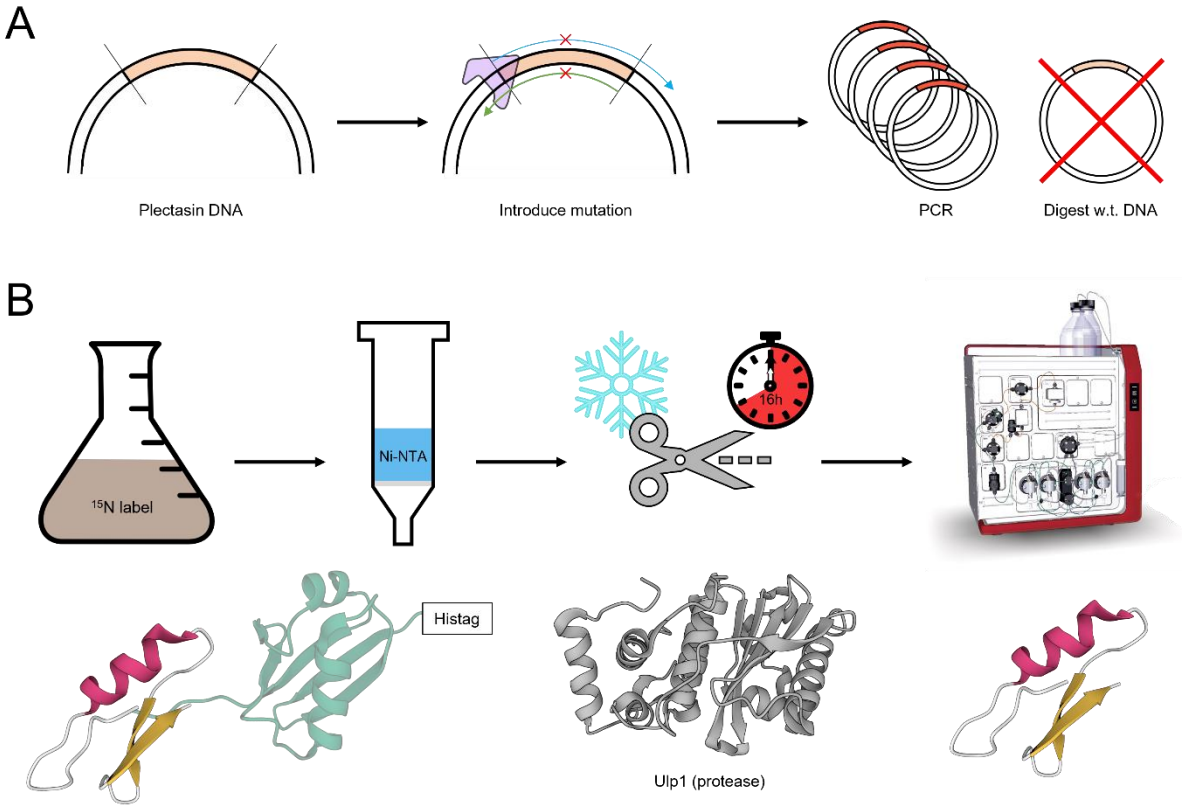

Figure 3. The schematic workflow of the production of plectasin. (A) Site-directed mutagenesis was used to turn wildtype plectasin DNA into the mutants that we wanted. This is done by a primer mismatch on both strands and amplification by PCR. The wildtype plectasin DNA was digested using a restriction enzyme specific for methylated sites. Plasmid stocks were obtained by transformation of *E. coli* DH5α and isolating the plasmids. (B) After transformation of *E. coli* Shuffle cells, they were grown in M9 minimal media containing $^{15}NH4Cl$. The cells were harvested 4 hours after induction and destroyed with a sonication probe. The His-tagged SUMO-plectasin was isolated using a Ni-NTA column, after which the SUMO was cleaved off by Ulp1 overnight. The mixture of proteins was purified using a gel-filtration column.

Materials and Methods

Plasmid construction
Plectasin DNA was inserted into pET_SUMO vector by previous PhD and MSc students. The construct contains the Small Ubiquitin-like Modifier (SUMO) protein as recombinant protein, which increases the solubility of plectasin in the cytosol and contains a his-tag for ease of purification.
Site-directed mutagenesis was performed on wildtype plectasin in the pET_SUMO with the primers that were provided (Table S1) using the KOD Hot Start DNA Polymerase protocol (Novagen)[36]. The thermocycles used were as follows: 1. 5:00 95 °C 2. 0:30 95 °C 3. 0:30 52 °C 4. 7:30 68 °C 5. Repeat steps 2-4 12x 6. 12:30 72 °C 7. 4 °C. Digestion of the wildtype vector was done using DpnI restriction enzyme, which only cuts methylated DNA.

Transformation of DH5α
Chemically competent *E. coli* DH5α was transformed using 10 µL of the PCR product following a standard heat shock protocol at 42 °C for 30 seconds. The bacteria were kept on ice and allowed to recover in SOC medium at 37 °C while shaking (200-250 rpm) for 1-2 hours. The bacteria were centrifuged at 3,000 × g for 2 minutes, resuspended in a small volume of supernatant (50 µl) and plated on a petri dish containing LB agar with 25 µg/ml kanamycin. The petri dishes were incubated overnight at 37 °C and afterwards put at 4 °C until needed.

Purification of the plasmid
Single colonies of transformed *E. coli* DH5α were inoculated into 5-10 mL LB containing 25 µg/mL kanamycin and grown overnight at 37 °C, 200 rpm. The plasmids were then isolated following a GeneJET Plasmid miniprep kit (#K0503, Thermo Scientific)[37]. The elution was done using Milli-Q (MQ) water. The plasmids were sent for Sanger sequencing (EZ-seq, Macrogen) according to their specifications. The resulting data was analysed using Serial Cloner v.2.6.1 and Macrogen's provided chromatograms.

Peptide expression and purification
SHuffle® T7 Express *lysY E. coli* (NEB) were transformed using 2 µl of purified plasmid DNA following the same protocol as above. *E. coli* Shuffle ® cells is a stain that facilitates the formation of disulfide bridges in the cytoplasm, which makes removes the otherwise necessary refolding of the protein. The LB agar was supplied with 25 µg/mL kanamycin and additionally 17.5 µg/ml chloramphenicol. The petri dishes were incubated overnight at 37 °C and afterwards put at 4 °C until needed.
Single colonies were inoculated into 1 ml LB containing 25 µg/ml kanamycin and 17.5 µg/ml chloramphenicol and incubated overnight at 37 °C while shaking at 200 rpm. The inoculates were diluted into 200 mL of M9 minimal medium and incubated at 37 °C while shaking overnight. The preculture was scaled up 1 L by diluting to OD_{600} 0.2-0.3 in (un)labelled M9 minimal medium and grown to OD_{600} 0.6. If isotopically labelled $^{15}NH_4Cl$ or ^{13}C-Glucose was used when scaling up, the preculture was first centrifuged at 3,000 × g for 10 minutes and the supernatant was discarded. The cells were resuspended in the labelled M9 medium. This was done to remove unlabelled material from the medium. The expression was induced by the addition of isopropyl ß-d-1 thiogalactopyranoside (IPTG) to a final concentration of 0.5 mM and incubated for 4 hours. The cells were harvested by centrifugation for 15 minutes at 4,000 × g at 4 °C and frozen at -20 °C in lysis buffer (50 mM sodium phosphate pH 8.0, 150 mM NaCl, 1 mM β-mercaptoethanol and 25 mM imidazole) until further use.
The cells were thawed and benzonase was added to the cell suspension. The bacteria were lysed by a sonication probe using intervals of 15/45 seconds on/off for 15 minutes. The sample was kept on ice during and after sonication to prevent the sample from heating up. The debris was centrifuged at 40,000 × g for 30 minutes and the supernatant was loaded onto a Ni-NTA column. The lysate was loaded onto the column four times, whereafter the column was washed using 10 CV of lysis buffer, and the SUMO-plectasin was eluted using 5 CV of elution buffer (50 mM phosphate buffer pH 8.0, 150 mM NaCl, 1 mM b-mercaptoethanol and 400 mM imidazole). The eluate was incubated with Ulp1 overnight at 4

°C, to cleave the bond between SUMO and plectasin. Verification of cleavage was done using tris/tricine SDS-PAGE (20%).
Plectasin was further purified using a gel-filtration column (Superdex 30 prep-grade HiLoad 260/60) on a Äkta pure system. The sample was loaded and eluted using buffer containing 50 mM Sodium phosphate, 150 mM NaCl and 1 mM b-mercaptoethanol. Purified plectasin was stored at -20 °C and was concentrated before use to avoid aggregation of the peptide. The sample concentration was done using an Amicon 15 Centrifugal Filter Units (3,000 NMWL). Buffer exchange was also done using Amicon Centrifugal Filter Units by dilution of the phosphate buffer to HEPES buffer of at least 600 times.

Solution NMR
All spectra shown were acquired using a Bruker 600 MHz spectrometer and analysed using Topspin 4.1.3 and Poky suite[38].
A 5 mm glass NMR tube (Wilmar) was filled with 20 µM ^{15}N-labelled plectasin in Pi buffer (50 mM NaPi, 150 mM NaCl, 1 mM β-mercaptoethanol) with 10% (v/v) D_2O. 2D NH heteronuclear single-quantum correlation (HSQC) experiments were acquired to assess the backbone fold. Assignments of the peaks were taken from literature[20,23,25,32].
Chemical shift perturbations (CSP) for the plectasin and the mutants free in solution can be calculated as the sum the absolute backbone H_N and N chemical shifts using:

$$\Delta\delta CSP, HN\ (ppm) = \sqrt{\frac{(\delta H, Plec - \delta H, Mut) + \left(\frac{\delta N, Plec - \delta N, Mut}{B}\right)^2}{2}}$$

where δH and δN are the chemical shifts (ppm) of the corresponding nuclei and B is the B-factor, which was kept as 5.

Isothermal titration calorimetry
Large unilamellar vesicles (LUVs) of DOPC, doped with 2% LII, were prepared using the extrusion method[39]. The concentration of the LUVs was determined as the concentration of inorganic phosphate after digestion with perchloric acid[40] by UV-VIS spectrometry. LUVs and plectasin w.t. or mutants (50 mM HEPES, 150 mM NaCl, 1 mM β-mercaptoethanol, pH 7.2) were degassed for 15 minutes at 37 °C prior to the start of the experiment. The cell was filled with 200 µL plectasin and 2 µL LUVs were titrated at set intervals at a rate of 0.5 µL/sec at a constant stirring rate of 125-150 rpm. All ITC measurements were performed at 37 °C on a Affinity ITC (TA Instruments). The resulting data was analysed using Nano Analyze Software (v.3.12.0, TA Instruments). Independent models were used for fitting of the raw data. As plectasin and its mutants cannot cross the membrane, the lipid II concentration was adjusted for the calculations.

Inhibitory assays
Antibacterial activity of plectasin and its mutants were determined using a broth microdilution assay according to the Clinical and Laboratory Standards Institute (CLSI) guidelines[41]. Colonies of MRSA (USA300), MSSA (ATCC29213) and *Staphylococcus simulans* were inoculated in cation-adjusted Müller-Hinton Broth (CAMHB) and grown overnight at 37 °C (non-shaking). The cultures were diluted OD_{600nm} 0.05 and grown to log phase (OD 0.1-0.3). The antibiotics were serially diluted in a round-bottom 96-well plate from a 100 µg/ml stock. The bacteria were added so the concentration was 10^6 CFU/ml. The plate was then incubated at 37 °C for 20 hours and growth was determined by eye. The experiments were performed in triplicate on different days and the average was recorded.
The inhibitory zone assay was performed using an overnight culture of bacteria, inoculating this into warm tryptic soy agar and pouring this into petri dishes to a height of 5 mm. Once cooled, 1000-125 nmol of plectasin and its mutants was spotted (~5µL) onto the agar. This was incubated 4 hours at 4 °C and another 24h at 37 °C. The size of the resulting disc was determined by scanning the plates and measuring using ImageJ.

Results

Production and purification of plectasin and mutants.

The pET_SUMO vectors containing the plectasin DNA were kindly provided by a previous PhD candidate and students. However, after the first round of protein expression and purification we concluded that some mutant vectors (M13L and M13L Q14R) did not contain correct mutation(s). For these mutants, vectors of plectasin were used for site-directed mutagenesis (Table S1). The product was introduced in *E. coli* DH5α and plasmids were isolated. The plasmid for every mutant was sequenced (Figure 4A) using Sanger sequencing. The correct mutations were identified in the plectasin sequence, while no other mutations were detected in either plectasin or SUMO. *E. coli* Shuffle® cells were transfected with the plectasin and mutant DNA. The Shuffle cell line allows for disulfide bridge formation in the cytoplasm of the bacteria, which is crucial for CSαβ defensins. After induction with IPTG, the cells were harvested and lysed. The SUMO-plectasin construct was purified with a Ni-NTA column and subsequently, the SUMO was cleaved of using Ulp1 (Figure 4B). The mixture was run over a gel-filtration column to purify plectasin (Figure 4C and D). Interestingly, the plectasin mutants containing D9N eluted later from the column. This suggests that these mutants adopt a smaller 3D conformation. Peaks 3-6 on the gel-filtration trace all contain plectasin (Figure 4D), however only plectasin from peak 6 is eluted as a monomeric state.

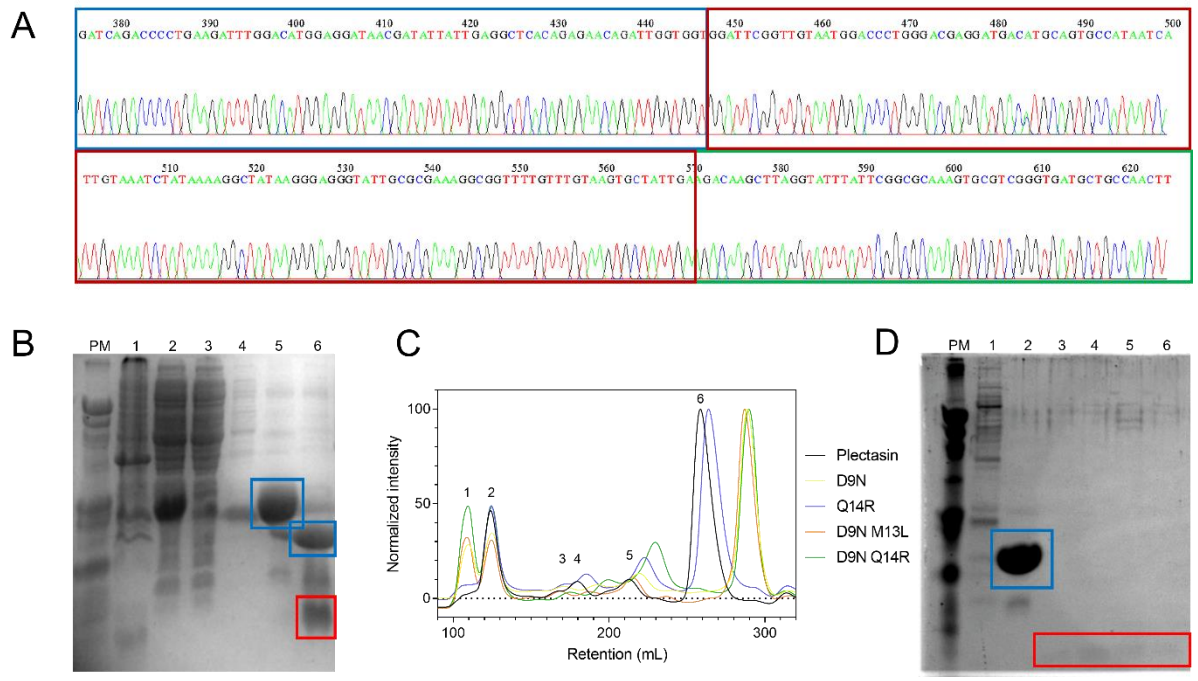

Figure 4. (A) Representative trace of sequenced plectasin DNA. It contains full length plectasin (red box), the SUMO protein (full length not shown, blue box) and the beginning of the pET_SUMO vector (green square). (B) Representative SDS-PAGE after the first purification on a Ni-NTA column. PM = protein marker. Loaded on the gel were the cell pellet after cell lysing (1), the supernatant (2), the flowthrough of the Ni-NTA column (3), the wash of the Ni-NTA column, the elution of the Ni-NTA column (5) and the elution after overnight cleavage of SUMO-plectasin using Ulp1 (6). In the red square was cleaved plectasin and in the blue squares are SUMO-plectasin (5) and SUMO (6). (C) Normalized gel-filtration UV traces of plectasin and the mutants D9N, Q14R, D9N M13L and D9N Q14R. Interestingly, the traces containing the D9N mutation elute later, thus are of a smaller particle size. Mutants M13L and M13L Q14R are excluded due to being run differently on the gel-filtration column. The numbers 1-6 correspond to the peaks of the plectasin trace. (D) Representative SDS-PAGE gel after gel-filtration. PM = protein marker. Loaded on the gel were 1-6 from the gel-filtration. Peak 2

contains the SUMO and peaks 3-6 all contain plectasin (red square), however only peak 6 is used for experiments.

Conserved protein fold with large chemical shift perturbations

We measured 2D N-H solution state NMR spectra of plectasin, NZ2114, and the mutants to ensure that the peptides folded correctly. All spectra could be fully assigned based on previous literature[20,22] (Table S2). Previous literature also mentioned several chemical shift perturbations (CSP) present in NZ2114 compared to plectasin[42,43], however the CSαβ-fold was conserved. We also observed the same CSPs (Figure 5A and S1) in NZ2114, where residues N5, W8, D/N9, E10, D11, D12 (negative patch) and M/L13 show huge signal shifts. Surprisingly, the single mutant D9N is the source of most of these perturbances (Fig 5B). N5, W8, E10, D11 and D12 all shift to a different state which is present for all mutants containing the D9N mutation. D9N is also the only mutation that causes relatively large perturbations further in the peptide, mainly for F35 and V36. CSPs per mutant are visualized in Fig. 6. Single mutant M13L shows perturbances in Q14 and itself, while Q14R only shows a shift in this residue. Interestingly, the M13L Q14R double mutant shows only a shift in the position of L13 and not R14. This is in accordance with the shifts present in NZ2114.

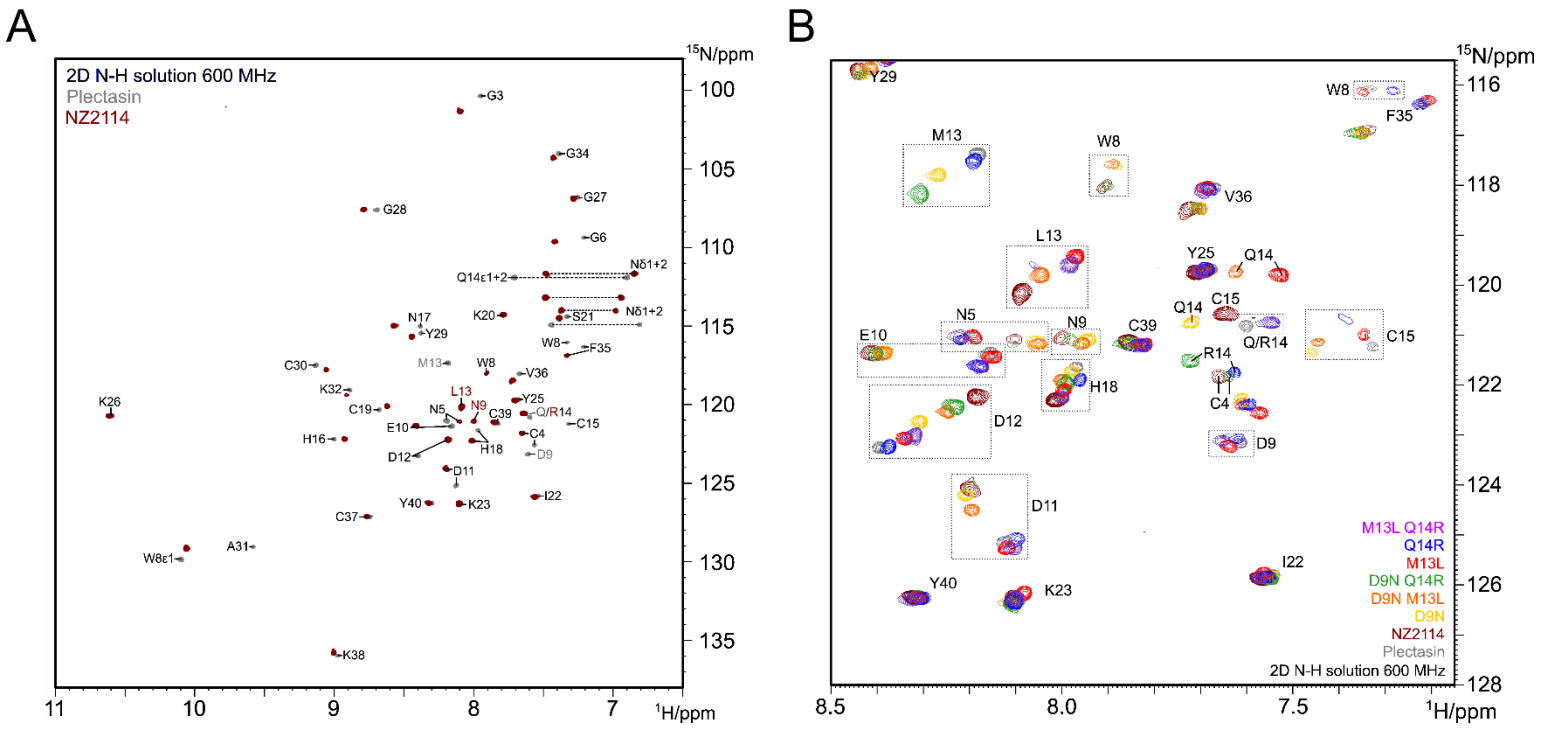

Figure 5. Comparison of 2D N-H NMR data of plectasin, NZ2114, and the mutants. (A) Overlay of the full spectra of plectasin and NZ2114. (B) Overlay of plectasin, NZ2114, and all the mutants in the region of interest of A. Additional regions of interested show the shifts of the anionic patch (D/N9-E10-D11-D12), M/L13, Q/R14, N5 and W8

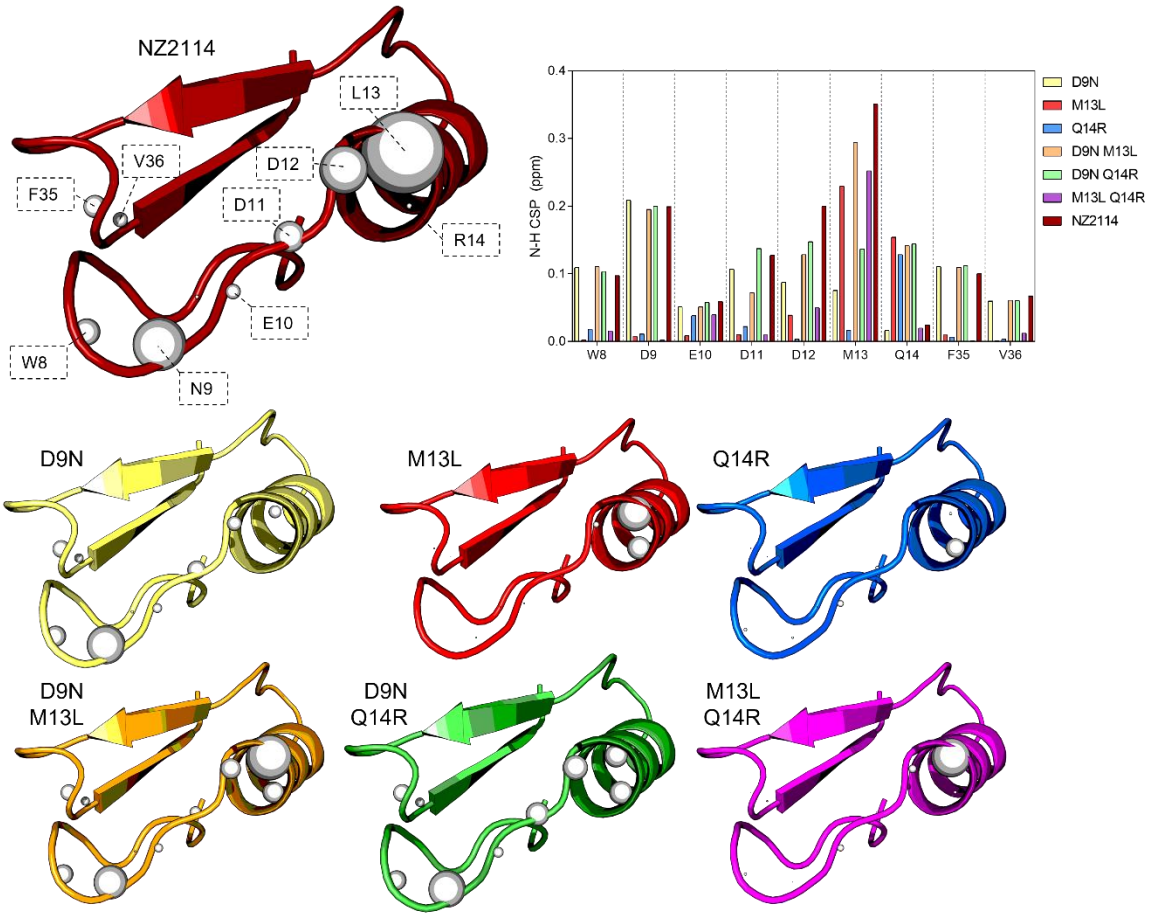

Figure 6. CSP of the negative patch and mutation sites visualised as white spheres in proportion with the perturbance measured in NMR compared to wildtype plectasin for NZ2114 and all mutants.

Mutations D9N and Q14R increased the antimicrobial activity

To investigate the importance the mutations had on the increased activity of NZ2114 against MRSA, we performed microbroth dilution assays were performed to determine the MIC for MRSA, methicillin-susceptible *Staphylococcus aureus* (MSSA) and *S. simulans* (SS). MSSA and SS were chosen as control strains to test if the activity of NZ2114 is selective for MRSA and for any *Staphylococcus.* None of the tested AMPs showed abolished inhibitory activity and all showed activity on par with or greater than wildtype plectasin (Table 1). For single mutants D9N and M13L, we observed no increase in MIC over plectasin, except for D9N against MSSA. Mutant Q14R showed an improvement in MIC against all tested bacteria, while the double mutant D9N Q14R performed on par with NZ2114. Surprisingly, the MIC for MRSA was lower than the MIC for MSSA for plectasin and all mutants except D9N. The combinations of D9N M13L and M13L Q14R did have increased antibacterial activity, however they showed the same amount of activity as the single mutant Q14R.

Our obtained MIC values for plectasin corresponded nicely to the literature (2-32 µg/ml[20,44]), whereas the MIC data for NZ2114 against MRSA were between 2-4 µg/ml for NZ2114[28,45], or previous in-house MIC data for NZ2114 (<0.78 µg/ml). Thus, we expected to see a greater difference between the mutants. As this was not the case, we opted to do a follow-up experiment to test the antimicrobial activity of the mutants.

Table 1. Minimal inhibitory concentrations (MIC), minimal bactericidal concentrations (MBC), and inhibition zone diameter of plectasin and its mutants against MRSA, MSSA and SS.

	MRSA		**MSSA**		**SS**	
	MIC (µg/ml)	size inhibition disc (mm)	MIC (µg/ml)	size inhibition disc (mm)	MIC (µg/ml)	size inhibition disc (mm)
Plectasin	12.5	8.8	25	7.3	12.5	13.1
D9N	12.5	10.1	12.5	8.1	12.5	13.3
M13L	12.5	8.8	25	7.9	12.5	13.1
Q14R	10.4	10.5	12.5	8.7	9.4	14.8
D9N M13L	10.4	10.4	12.5	8.6	6.3	13.7
D9N Q14R	8.3	11.7	12.5	9.6	6.3	15.2
M13L Q14R	10.4	11.3	12.5	9.0	9.4	14.5
NZ2114	8.3	11.6	12.5	9.7	6.3	14.7
Vancomycin	0.8	-	0.8	-	0.8	-

Additionally, an inhibition zone assay was performed to assess the inhibitory efficacy of plectasin (Fig. 7, Table 1) in the hope to find a greater discrepancy between the different mutant activities. The size of the disc corresponds to the area of growth inhibited bacteria and a greater area means greater bactericidal activity. As expected, the inhibition was most limited for the wildtype plectasin, with the M13L mutant having similar antimicrobial activity. We could now differentiate the effectiveness between D9N and Q14R, as the latter had a greater disc size. The double mutants follow the same trend, as the D9N Q14R was close to or sometimes even outperforming NZ2114. M13L Q14R was slightly worse, but still outperformed D9N M13L. These trends were observed against MRSA and also MSSA and *S. simulans* (Table S3; Figure S2).

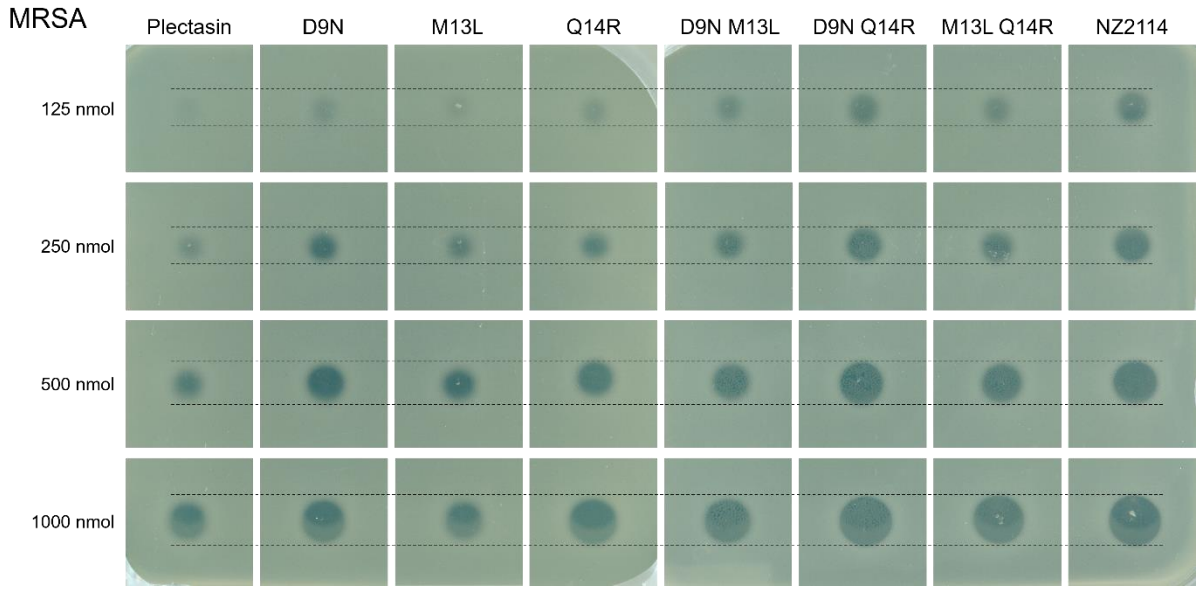

Figure 7. Inhibition zone assay of plectasin and its mutants on MRSA. The size of the discs are shown in Table 1. The bacteria are allowed to grow inside the agar medium while 125, 250, 500 and 1,000 nmol (5 µL) of the AMPs are added on top op the agar. This was then incubated for 20 hours and a scan

was made of the agar plate. The sizes of the discs of 1000 nmol plectasin are in Table 1, all values are in Table S3.

The thermodynamic profile of D9N and M13L mutants was similar to NZ2114

We compared binding affinities (K_d, Figure 8) and thermodynamic parameters (ΔG, ΔH, TΔS, Table 2) of plectasin, NZ2114 and our mutants with LII doped DOPC LUVs using isothermal titration calorimetry (ITC). In this system, plectasin should only have had access to 1% LII, due to it being unable to cross the membrane and access the inner leaflet. Wildtype plectasin had a high entropy and high enthalpy value, while NZ2114 had an entropy of close to zero and the binding energy coming almost entirely from enthalpy. We found that the strongest binder (lowest K_d) to LII was the M13L mutant. We expected to see the same high entropy as we saw for the wildtype plectasin, due to the mutation not improving the MIC. While still having a slightly higher entropy than the other mutants with the exception of Q14R, the thermodynamic profile of M13L more closely resembled NZ2114 . This was also the case for D9N and the double mutants of D9N, but this was expected due to the CSPs we observed during the NMR experiments. All double mutants performed similarly to each other, while D9N M13L plectasin had a slightly higher K_d than D9N Q14R and M13L Q14R. Remarkably, while the K_d of Q14R plectasin was the worst out of all our mutants, its thermodynamic profile matches that of plectasin and it had an increased antimicrobial effect.

Table 2. Thermodynamic parameters (Kd, ΔG, ΔH and -TΔS) for the binding of plectasin and its mutants to LII (2%) doped DOPC LUVs.

	K_d (M)	ΔG (kJ/mol)	ΔH (kJ/mol)	-TΔS (kJ/mol)
Plectasin	4.56E-06	-31.71	-79.04	47.33
D9N	8.51E-07	-36.04	-32.89	-3.154
M13L	6.10E-08	-42.84	-51.8	8.957
Q14R	1.00E-04	-23.75	-80.26	56.51
D9N M13L	3.22E-06	-32.61	-33.07	0.458
D9N Q14R	1.42E-06	-34.73	-26.59	-8.137
M13L Q14R	1.89E-06	-33.99	-25.02	-8.962
NZ2114	2.86E-06	-32.92	-33.52	0.602

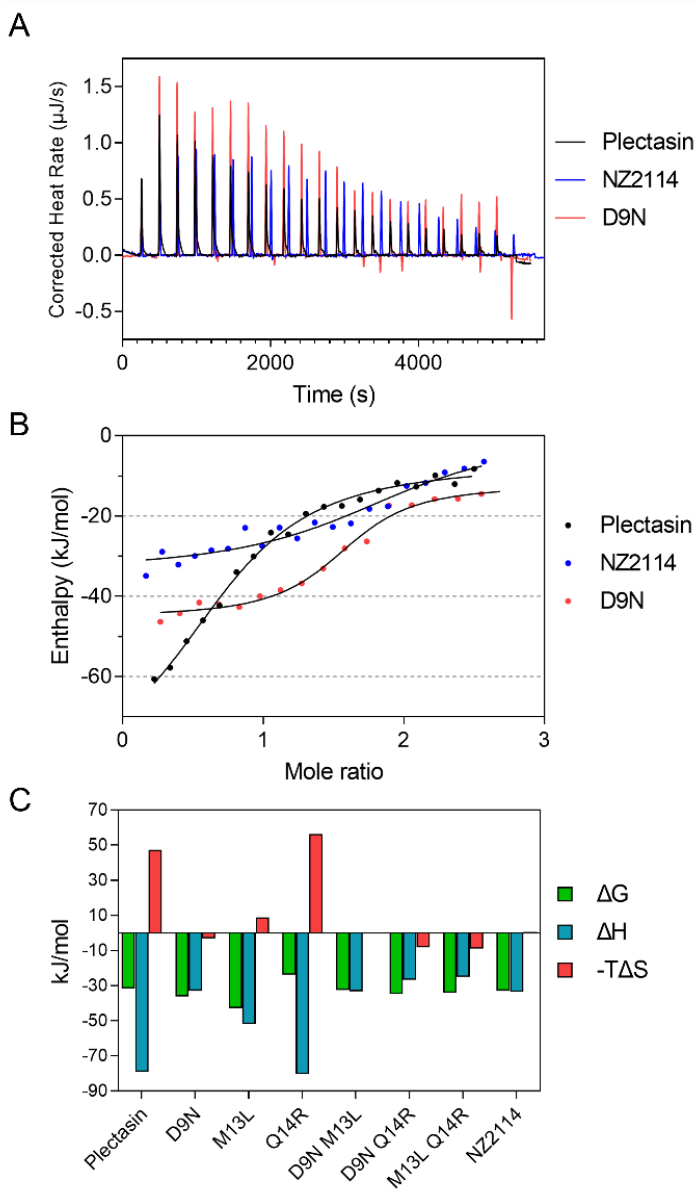

Figure 8. Representative isothermal titration calorimetry (ITC) data. (A) The corrected heat release data of plectasin, NZ2114 and D9N. (B) The enthalpy measured in A is plotted against the mole ratio of the added LUVs. (C) The thermodynamic parameters of plectasin and the mutants (see Table 2 also). ITC measurements were performed 1-3 times for each peptide.

Discussion

Conclusion

The major advantage NZ2114 has over plectasin is its effectiveness again MRSA. The difference between NZ2114 and wildtype plectasin are the mutations D9N, M13L and Q14R. These mutations do not overlap with the proposed binding site to LII, but are close to the plectasin specific anionic patch, which is the proposed divalent cation binding site. Here, we looked at the influence these mutations (single and double mutants) had on the effectiveness of plectasin in antimicrobial activity and binding LII and its structure. We could already see during the purification that the D9N mutation caused small changes in the conserved CSαβ defensin fold. With NMR, we could see that this mutation perturbs the whole anionic patch (D/N9-E10-D11-D12) of plectasin, while the single and double mutants of M13L and Q14R only show very small chemical shift perturbations in the α-helix (M13-S21). We could clearly observe an increase in the MIC for the mutants D9N, Q14R and their double mutant, which has around the same potency as NZ2114. The single mutant M13L did not improve its activity, however the double mutants of M13L did have better activity over the single mutant. The LII binding affinity for plectasin and NZ2114 was around the same strength, while mutations D9N and M13L increased the binding affinity by 5 and 100 fold. Furthermore, we observed a decrease in binding affinity for Q14R by 200 fold, while its thermodynamic parameters (ΔH and TΔS) stayed comparable with those of plectasin with a high entropy and enthalpy values. The thermodynamic parameters of the D9N and M13L single and double mutants showed a closer resemblance to NZ2114, with lower entropy values close to zero.

Discussion

Previous research by this group[25] suggests that residues D9, M13 and Q14 are not part of the binding interface of the plectasin-LII complex. However, we see a very large contribution of the D9N mutation to the protein conformation based on NMR data. The mutations allosterically perturbs residues W8 and F35, as seen in the NMR data (Figure 5, 9A and S1), which are part of the binding interface of LII-plectasin. We suggest based on this and previous studies that the mutation D9N induces a change in the conformation that allows for plectasin to bind a wider array of LII isoforms. This includes the heavily modified LII of MRSA. We speculate that the amidation of E2 and/or the addition of a pentaglycine peptide on K3 might lead to a loss of interaction between LII and wildtype plectasin. This would be supported by the ITC data above, as the mutants of D9N and NZ2114 do not have to overcome a large entropic penalty, thus needing less binding interactions with LII.

Mutations D9N and Q14R also replace the negatively charged aspartic acid for asparagine and a glutamine for a positively charged arginine. Both mutations are located in or close to the extremely negatively charged part of plectasin. These mutations radically change the charge in plectasin, from +1 to +3 overall. This more positively charged plectasin is highly likely to be less repelled by the great amount of negatively charged lipids (phosphatidyl glycerol and cardiolipin) in the bacterial membrane[46].

Mutations M13L and Q14R do not cause CSPs in the Ca^{2+} or LII binding site, but rather in the α-helix. Residue H18 in present in the α-helix and likely involved in the oligomerization of plectasin[22]. The process of oligomerization is driven by the hydrophobic effect and is part of the entropic penalty. While Q14R has a large entropic contribution, the double mutant M13L Q14R does not anymore. Thus, we expect the M13L and Q14R mutations to improve the bacteriostatic activity of NZ2114 by improved oligomerization and the mutations D9N and Q14R to improve the binding to bacterial membrane by the charge difference.

Other plectasin derivatives (NZ2114[29], MP1102[30] and Py4[31]) had their Q14 replaced by a positively charged residues (R and K). All these mutants and our studied Q14R single and double mutants all have increased activity towards MRSA over plectasin. Interestingly, the Q14R single mutant is the only mutant that shows a similar thermodynamic profile (Figure 8C) as plectasin in our ITC studies and had the same retention time as wildtype plectasin in our gel-filtration (Figure 4C). Plectasin and the Q14R mutant have an bigger conformation than the D9N mutant. We think this is due to plectasin being in a partially unfolded structure, due their different thermodynamic profile compared to NZ2114 and the D9N mutants.

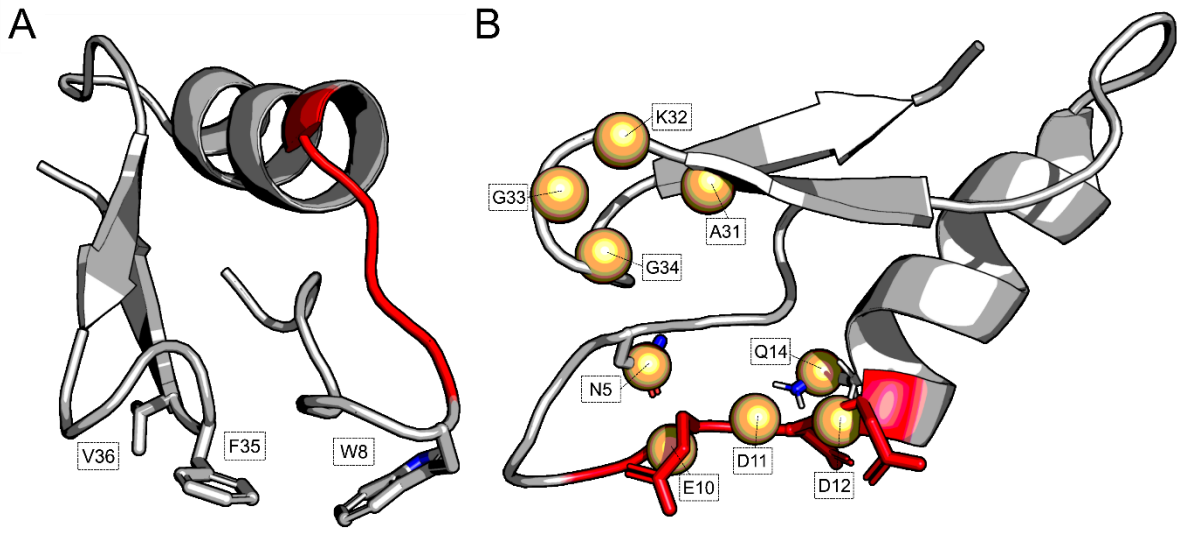

Figure 9. Wildtype plectasin. (A) Residues D9, M13 and Q14 are coloured red and residues W8 and F35 are visualized as sticks. (B) Plectasin with the anionic patch coloured red and the residues involved in the Ca^{2+} binding visualized as yellow spheres.

The role Ca^{2+} plays in the mode of action of plectasin is more significant then was assumed at the start of this study. Plectasin binds to divalent cations with the anionic patch (E10-D12), the β-loop (A31-G34) and side chains of N5 and Q14[25] (Figure 9B). Ca^{2+} is the strongest binder[23], however the effect of Ca^{2+} on the mode of action of plectasin remains elusive. We have observed Ca^{2+} dependency in LII doped DOPC vesicles in which there is no permeabilization effect in the absence of free Ca^{2+} (unpublished data, Maik Derks). It has been shown that plectasin can bind LII in the absence of Ca^{2+}[47], thus Ca^{2+} seems to only be necessary for the permeabilization of the membrane.
The D9N mutation also disturbs the Ca^{2+} binding site consisting of D-x-D, that is a conserved sequence in other types of antibiotics, like lipopeptides[48,49] and mutation D9N and Q14R also decrease the negative charges in and around the anionic patch. The latter may lead to a independence of Ca^{2+} or enhanced effect when bound to Ca^{2+} for NZ2114 in its mode of action, however this needs to be investigated. Preliminary data shows that NZ2114 has a lower affinity (K_d) for Ca^{2+} than plectasin has[23] and it was observed that NZ2114 changes conformation upon binding Ca^{2+}[23]. This Ca^{2+} dependence could explain the large variance in ITC data we acquired and the multiple states of plectasin and NZ2114 in previous NMR experiments[23]. In this and previous studies, Ca^{2+} was often not added to the system during the NMR and ITC experiments. Plectasin strongly binds divalent ions, e.g. Ca^{2+}, Mg^{2+} or Ni^{2+}, and these cations may be present in differing amounts in the stock solutions, which were not removed during the production and purification. Other CSαβ defensins, like insect defensin[50], plant defensins[51] and ASABF[52], show a decrease in killing activity with increasing Ca^{2+} concentrations. We suggest that this is caused by a high concentration of Ca^{2+} leading to more ions bound to the lipid surface and increasing the tightness of the lipid packing, thus creating more difficulty for plectasin to bind LII[53,54]. This Ca^{2+} dependency of plectasin should always be considered in experiments to come and previous studies and data about plectasin without Ca^{2+} should be reassessed.

As mentioned in the results section, our MIC results for NZ2114 did not closely correspond to data from this and other groups. While we saw an increase in MIC for NZ2114 over plectasin, this was only a 2 fold increase, while literature reports a 10-25 fold increase[20,25,28,44,45]. The differences between plectasin and the mutants became more clear with the inhibition zone assay, still do not represent the dramatic increase we can see in the literature. The reason for why the MIC measurements do not show a large difference between plectasin and NZ2114 in this study remains unknown, but we can speculate. The first and most obvious cause: there could be a error in the stock. NZ2114 was the only stock not specifically prepared for this study, the other peptides were. For the preparation of the stocks in the

MIC and IZA experiments, the concentration of NZ2114 and all other plectasins were measured using a Nanodrop 2000 spectrophotometer. No mistakes were found here. The peptides were diluted in the same stock of PBS before the MIC experiments, if there went something wrong with this, we would have seen a difference for the other mutants too during the MIC determination. The MIC determination was also done in triplicate to ensure an authentic result. Lastly, the mutation might cause plectasin to aggregate out of solution more easily[55], as mentioned above, however we did not observe formation of a precipitate after preparation of the stocks for MIC determination.

Future prospects

Next steps in understanding plectasin and derivatives include having (labelled) MRSA-LII. This LII contains an amidated E2[34] on the pentapeptide and a pentaglycine on the K3[35]. These modifications are crucial for the AMR of MRSA and it is crucial to know how plectasin and especially NZ2114 interacts with this LII.. This can be investigated using a ssNMR approach with MRSA-LII doped liposomes. We should be able to see contacts between wildtype plectasin and the E2, that would disappear with the amidated E2. The plectasin residues in contact with E2 should be one of the three residues mutated in NZ2114 or one of the residues that undergoes a CSP due to the D9N mutation. This would give a better understanding of the plectasin-LII interface, which could afterwards be modelled with the newly obtained restraints in a LII doped bilayer system.

Oligomerization seem to be an important mode of action of antimicrobial peptides in general. Many have been observed to be able to oligomerize and kill bacteria in this way, e.g. teixobactin[18], nisin[56] and protegrin-I[57]. While this group has been able to determine some contacts in plectasin-LII and plectasin-plectasin complexes, the overall structure and mode of action is still obscured. There are multiple models for the modes of action of AMPs[58], however the two main hypothesizes are pore formation and metabolic inhibition. Pore formation or membrane permeabilization can be achieved in a multitude of ways[59] (toroid pore, barrel-stave, carpet and aggregate models), but it is difficult to determine what is actually happening on the surface of a membrane. Two ways to further investigate this are high-speed atomic force microscopy (HS-AFM) and cryo-electron tomography (cryo-ET). HS-AFM would allow for the investigation of pore formation in model systems containing LII or biological membrane (from membrane isolate)[60,61]. Cryo-ET would give insight in the oligomeric state of the plectasin-plectasin complex and can possibly provide structure at atomic resolution[62,63].

Lastly, Ca^{2+} plays a vital role in the mode of action of plectasin and . From research done in this group, Ca^{2+} is needed permeabilization of the membrane. The residues that can interact with these cations have been determined with the use of paramagnetic divalent cation Mn^{2+}[25]. A ssNMR study using a Ca^{2+} probe can verify these contacts and find contacts of Ca^{2+} with the membrane. Hopefully, a structure of bound LII-plectasin with Ca^{2+} can be obtained to elucidate the complex and their interaction.

Acknowledgements

I would like to thank Markus Weingarth, PhD for giving me the opportunity to help with this project and to gain experience in the field of antibiotics and biological NMR. Maik Derks, MSc was a great guide and help for learning the techniques to be able to perform this research. Shehrazade 'Miranda' Jekhmane, PhD, Benjamin Vermeer, MSc and Vicky Charitou, MSc for their previous work on the project, providing materials and plasmids as well as protocol and lab journals for when problems were encountered. Edwin Veldhuizen, PhD and his PhD candidate Ali Javed, MSc kindly provided the ML-II lab space and techniques for working with MRSA and also providing access to their ITC machine, which briefly used due to some difficulties, but no results shown here were obtained from. Rhythm Shukla, MSc was a great help with the troubles that arose with the ITC machine.

References

(1) Murray, C. J.; Ikuta, K. S.; Sharara, F.; Swetschinski, L.; Robles Aguilar, G.; et al. Global Burden of Bacterial Antimicrobial Resistance in 2019: A Systematic Analysis. *Lancet* **2022**, *399* (10325), 629–655. https://doi.org/10.1016/S0140-6736(21)02724-0.

(2) Cassini, A.; Högberg, L. D.; Plachouras, D.; Quattrocchi, A.; Hoxha, A.; et al. Attributable Deaths and Disability-Adjusted Life-Years Caused by Infections with Antibiotic-Resistant Bacteria in the EU and the European Economic Area in 2015: A Population-Level Modelling Analysis. *Lancet Infect. Dis.* **2019**, *19* (1), 56–66. https://doi.org/10.1016/S1473-3099(18)30605-4.

(3) World Health Organization. *Antibacterial Agents in Clinical and Preclinical Development: An Overview and Analysis*; 2021.

(4) Lewis, K. The Science of Antibiotic Discovery. *Cell* **2020**, *181* (1), 29–45. https://doi.org/10.1016/j.cell.2020.02.056.

(5) Livermore, D. M.; Blaser, M.; Carrs, O.; Cassell, G.; Fishman, N.; et al. Discovery Research: The Scientific Challenge of Finding New Antibiotics. *J. Antimicrob. Chemother.* **2011**, *66* (9), 1941–1944. https://doi.org/10.1093/jac/dkr262.

(6) Renwick, M. J.; Brogan, D. M.; Mossialos, E. A Systematic Review and Critical Assessment of Incentive Strategies for Discovery and Development of Novel Antibiotics. *J. Antibiot. (Tokyo).* **2016**, *69* (2), 73–88. https://doi.org/10.1038/ja.2015.98.

(7) Luepke, K. H.; Mohr, J. F. The Antibiotic Pipeline: Reviving Research and Development and Speeding Drugs to Market. *Expert Rev. Anti. Infect. Ther.* **2017**, *15* (5), 425–433. https://doi.org/10.1080/14787210.2017.1308251.

(8) OECD; WHO; FAO; OIE. Tackling Antimicrobial Resistance Ensuring Sustainable R&D. *http://www.oecd.org/g20/summits/hamburg/Tackling-Antimicrobial-Resistance-Ensuring-Sustainable-RD.pdf* **2017**.

(9) Tacconelli, E.; Carrara, E.; Savoldi, A.; Harbarth, S.; Mendelson, M.; et al. Discovery, Research, and Development of New Antibiotics: The WHO Priority List of Antibiotic-Resistant Bacteria and Tuberculosis. *Lancet Infect. Dis.* **2018**, *18* (3), 318–327. https://doi.org/10.1016/S1473-3099(17)30753-3.

(10) IACG. *No Time To Wait: Securing the Future From Drug-Resistant Infections Report To the Secretary-General of the United Nations*; 2019.

(11) IACG. *No Time To Wait: Securing the Future From Drug-Resistant Infections Report To the Secretary-General of the United Nations*; 2019.

(12) Breukink, E.; de Kruijff, B. Lipid II as a Target for Antibiotics. *Nat. Rev. Drug Discov.* **2006**,

5 (4), 321–323. https://doi.org/10.1038/nrd2004.

(13) Egan, A. J. F.; Errington, J.; Vollmer, W. Regulation of Peptidoglycan Synthesis and Remodelling. *Nat. Rev. Microbiol.* **2020**, *18* (8), 446–460. https://doi.org/10.1038/s41579-020-0366-3.

(14) Müller, A.; Klöckner, A.; Schneider, T. Targeting a Cell Wall Biosynthesis Hot Spot. *Nat. Prod. Rep.* **2017**, *34* (7), 909–932. https://doi.org/10.1039/C7NP00012J.

(15) de Kruijff, B.; van Dam, V.; Breukink, E. Lipid II: A Central Component in Bacterial Cell Wall Synthesis and a Target for Antibiotics. *Prostaglandins Leukot. Essent. Fat. Acids* **2008**, *79* (3–5), 117–121. https://doi.org/10.1016/j.plefa.2008.09.020.

(16) Oppedijk, S. F.; Martin, N. I.; Breukink, E. Hit 'em Where It Hurts: The Growing and Structurally Diverse Family of Peptides That Target Lipid-II. *Biochim. Biophys. Acta - Biomembr.* **2016**, *1858* (5), 947–957. https://doi.org/10.1016/j.bbamem.2015.10.024.

(17) Levine, D. P. Vancomycin: A History. *Clin. Infect. Dis.* **2006**, *42* (Supplement_1), S5–S12. https://doi.org/10.1086/491709.

(18) Shukla, R.; Medeiros-Silva, J.; Parmar, A.; Vermeulen, B. J. A.; Das, S.; et al. Mode of Action of Teixobactins in Cellular Membranes. *Nat. Commun.* **2020**, *11* (1), 2848. https://doi.org/10.1038/s41467-020-16600-2.

(19) Breukink, E.; De Kruijff, B. The Lantibiotic Nisin, a Special Case or Not? *Biochim. Biophys. Acta - Biomembr.* **1999**, *1462* (1–2), 223–234. https://doi.org/10.1016/S0005-2736(99)00208-4.

(20) Mygind, P. H.; Fischer, R. L.; Schnorr, K. M.; Hansen, M. T.; Sönksen, C. P.; et al. Plectasin Is a Peptide Antibiotic with Therapeutic Potential from a Saprophytic Fungus. *Nature* **2005**, *437* (7061), 975–980. https://doi.org/10.1038/nature04051.

(21) Schneider, T.; Kruse, T.; Wimmer, R.; Wiedemann, I.; Sass, V.; et al. Plectasin, a Fungal Defensin, Targets the Bacterial Cell Wall Precursor Lipid II. *Science (80-.).* **2010**, *328* (5982), 1168–1172. https://doi.org/10.1126/science.1185723.

(22) Jekhmane, S. Solid-State NMR Studies on Therapeutic Peptides, Utrecht University, 2020.

(23) Charitou, V. Effect of Divalent Ions on the Antimicrobial Peptide Plectasin and Its MRSA-Active Derivative NZ2114, University Utrecht, Bijvoet Centre for Biomolecular Research, NMR spectroscopy, 2021.

(24) Medeiros-Silva, J.; Jekhmane, S.; Paioni, A. L.; Gawarecka, K.; Baldus, M.; et al. High-Resolution NMR Studies of Antibiotics in Cellular Membranes. *Nat. Commun.* **2018**, *9* (1). https://doi.org/10.1038/S41467-018-06314-X.

(25) Jekhmane, S. *Solid-State NMR Studies on Therapeutic Peptides*; 2020.

(26) Wilmes, M.; Cammue, B. P. A.; Sahl, H.-G.; Thevissen, K. Antibiotic Activities of Host Defense Peptides: More to It than Lipid Bilayer Perturbation. *Nat. Prod. Rep.* **2011**, *28* (8), 1350. https://doi.org/10.1039/c1np00022e.

(27) Xiang, F.; Xie, Z.; Feng, J.; Yang, W.; Cao, Z.; et al. Plectasin, First Animal Toxin-Like Fungal Defensin Blocking Potassium Channels through Recognizing Channel Pore Region. *Toxins (Basel).* **2015**, *7* (1), 34–42. https://doi.org/10.3390/toxins7010034.

(28) Brinch, K. S.; Tulkens, P. M.; Van Bambeke, F.; Frimodt-Moller, N.; Hoiby, N.; Kristensen, H.-H. Intracellular Activity of the Peptide Antibiotic NZ2114: Studies with Staphylococcus Aureus and Human THP-1 Monocytes, and Comparison with Daptomycin and Vancomycin. *J. Antimicrob. Chemother.* **2010**, *65* (8), 1720–1724. https://doi.org/10.1093/jac/dkq159.

(29) Andes, D.; Craig, W.; Nielsen, L. A.; Kristensen, H. H. In Vivo Pharmacodynamic Characterization of a Novel Plectasin Antibiotic, NZ2114, in a Murine Infection Model. *Antimicrob. Agents Chemother.* **2009**, *53* (7), 3003–3009. https://doi.org/10.1128/AAC.01584-08.

(30) Zhang, Y.; Teng, D.; Wang, X.; Mao, R.; Cao, X.; et al. In Vitro and in Vivo Characterization of a New Recombinant Antimicrobial Peptide, MP1102, against Methicillin-Resistant Staphylococcus Aureus. *Appl. Microbiol. Biotechnol.* **2015**, *99* (15), 6255–6266. https://doi.org/10.1007/S00253-015-6394-7.

(31) Qi, S.; Gao, B.; Zhu, S. A Fungal Defensin Inhibiting Bacterial Cell-Wall Biosynthesis with Non-Hemolysis and Serum Stability. *J. Fungi* **2022**, *8* (2). https://doi.org/10.3390/jof8020174.

(32) Vermeer, B. Differences in Target Binding Mode of Antibiotic Peptide Plectasin and Its MRSA-Active Derivative NZ2114, University Utrecht, Bijvoet Centre for Biomolecular Research, NMR spectroscopy, 2019.

(33) Pohl, C.; Zalar, M.; Bialy, I. El; Indrakumar, S.; Peters, G. H. J.; et al. The Effect of Point Mutations on the Biophysical Properties of an Antimicrobial Peptide: Development of a Screening Protocol for Peptide Stability Screening. *Mol. Pharm.* **2020**, *17* (9), 3298–3313. https://doi.org/10.1021/acs.molpharmaceut.0c00406.

(34) Münch, D.; Roemer, T.; Lee, S. H.; Engeser, M.; Sahl, H. G.; Schneider, T. Identification and in Vitro Analysis of the GatD/MurT Enzyme-Complex Catalyzing Lipid II Amidation in Staphylococcus Aureus. *PLoS Pathog.* **2012**, *8* (1), 1–11. https://doi.org/10.1371/journal.ppat.1002509.

(35) Schneider, T.; Senn, M. M.; Berger-Bächi, B.; Tossi, A.; Sahl, H. G.; Wiedemann, I. In Vitro Assembly of a Complete, Pentaglycine Interpeptide Bridge Containing Cell Wall Precursor (Lipid II-Gly5) of Staphylococcus Aureus. *Mol. Microbiol.* **2004**, *53* (2), 675–685. https://doi.org/10.1111/j.1365-2958.2004.04149.x.

(36) Novagen. Hot Start DNA Polymerase. In *The Dictionary of Genomics, Transcriptomics and Proteomics*; Wiley-VCH Verlag GmbH & Co. KGaA: Weinheim, Germany, 2015; pp 1–1. https://doi.org/10.1002/9783527678679.dg05760.

(37) Therme Scientific. Thermo Scientific GeneJET Plasmid Miniprep Kit. *Manual* **2014**, 1–9.

(38) Lee, W.; Rahimi, M.; Lee, Y.; Chiu, A. POKY: A Software Suite for Multidimensional NMR and 3D Structure Calculation of Biomolecules. *Bioinformatics* **2021**, *37* (18), 3041–3042. https://doi.org/10.1093/bioinformatics/btab180.

(39) Hope, M. J.; Bally, M. B.; Webb, G.; Cullis, P. R. Production of Large Unilamellar Vesicles by a Rapid Extrusion Procedure. Characterization of Size Distribution, Trapped Volume and Ability to Maintain a Membrane Potential. *Biochim. Biophys. Acta - Biomembr.* **1985**, *812* (1), 55–65. https://doi.org/10.1016/0005-2736(85)90521-8.

(40) Rouser, G.; Fleischer, S.; Yamamoto, A. Two Dimensional Thin Layer Chromatographic Separation of Polar Lipids and Determination of Phospholipids by Phosphorus Analysis of Spots. *Lipids* **1970**, *5* (5), 494–496. https://doi.org/10.1007/BF02531316.

(41) CLSI. *Methods for Dilution Antimicrobial Susceptibility Tests for Bacteria That Grow Aerobically ; Approved Standard — Ninth Edition*; 2012; Vol. 32.

(42) Li, Z.; Wang, X.; Wang, X.; Teng, D.; Mao, R.; et al. Research Advances on Plectasin and Its Derivatives as New Potential Antimicrobial Candidates. *Process Biochem.* **2017**, *56* (12), 62–70. https://doi.org/10.1016/j.procbio.2017.02.006.

(43) Pohl, C.; Zalar, M.; Bialy, I. El; Indrakumar, S.; Peters, G. H. J.; et al. The Effect of Point Mutations on the Biophysical Properties of an Antimicrobial Peptide: Development of a

Screening Protocol for Peptide Stability Screening. *Mol. Pharm.* **2020**, *17* (9), 3298–3313. https://doi.org/10.1021/acs.molpharmaceut.0c00406.

(44) Yang, Y.; Teng, D.; Zhang, J.; Tian, Z.; Wang, S.; Wang, J. Characterization of Recombinant Plectasin: Solubility, Antimicrobial Activity and Factors That Affect Its Activity. *Process Biochem.* **2011**, *46* (5), 1050–1055. https://doi.org/10.1016/j.procbio.2011.01.018.

(45) Chen, H.; Mao, R.; Teng, D.; Wang, X.; Hao, Y.; et al. Design and Pharmacodynamics of Recombinant NZ2114 Histidine Mutants with Improved Activity against Methicillin-Resistant Staphylococcus Aureus. *AMB Express* **2017**, *7* (1), 46. https://doi.org/10.1186/s13568-017-0345-x.

(46) O'Leary, W. M.; Wilkinson, S. G. Gram Positive Bacteria. In *Microbial Lipids*; Ratledge, C., Wilkinson, S. G., Eds.; Academic Press, 1988; pp 117–201.

(47) Ammerlaan, D. Exploring Metal Binding to the Antimicrobial Peptide Plectasin, Utrecht University, 2019.

(48) Hover, B. M.; Kim, S.-H.; Katz, M.; Charlop-Powers, Z.; Owen, J. G.; et al. Culture-Independent Discovery of the Malacidins as Calcium-Dependent Antibiotics with Activity against Multidrug-Resistant Gram-Positive Pathogens. *Nat. Microbiol.* **2018**, *3* (4), 415–422. https://doi.org/10.1038/s41564-018-0110-1.

(49) Wood, T. M.; Martin, N. I. The Calcium-Dependent Lipopeptide Antibiotics: Structure, Mechanism, & Medicinal Chemistry. *Medchemcomm* **2019**, *10* (5), 634–646. https://doi.org/10.1039/c9md00126c.

(50) Cociancich, S.; Ghazi, A.; Hetru, C.; Hoffmann, J. A.; Letellier, L. Insect Defensin, an Inducible Antibacterial Peptide, Forms Voltage-Dependent Channels in Micrococcus Luteus. *J. Biol. Chem.* **1993**, *268* (26), 19239–19245. https://doi.org/10.1016/s0021-9258(19)36505-6.

(51) Osborn, R. W.; De Samblanx, G. W.; Thevissen, K.; Goderis, I.; Torrekens, S.; et al. Isolation and Characterisation of Plant Defensins from Seeds of Asteraceae, Fabaceae, Hippocastanaceae and Saxifragaceae. *FEBS Lett.* **1995**, *368* (2), 257–262. https://doi.org/10.1016/0014-5793(95)00666-W.

(52) Zhang, H.; Yoshida, S.; Aizawa, T.; Murakami, R.; Suzuki, M.; et al. In Vitro Antimicrobial Properties of Recombinant ASABF, an Antimicrobial Peptide Isolated from the Nematode Ascaris Suum. *Antimicrob. Agents Chemother.* **2000**, *44* (10), 2701–2705. https://doi.org/10.1128/AAC.44.10.2701-2705.2000.

(53) Melcrová, A.; Pokorna, S.; Pullanchery, S.; Kohagen, M.; Jurkiewicz, P.; et al. The Complex Nature of Calcium Cation Interactions with Phospholipid Bilayers. *Sci. Rep.* **2016**, *6* (1), 38035. https://doi.org/10.1038/srep38035.

(54) Deplazes, E.; Tafalla, B. D.; Murphy, C.; White, J.; Cranfield, C. G.; Garcia, A. Calcium Ion Binding at the Lipid–Water Interface Alters the Ion Permeability of Phospholipid Bilayers. *Langmuir* **2021**, *37* (48), 14026–14033. https://doi.org/10.1021/acs.langmuir.1c02016.

(55) Pohl, C.; Effantin, G.; Kandiah, E.; Meier, S.; Zeng, G.; et al. PH- and Concentration-Dependent Supramolecular Assembly of a Fungal Defensin Plectasin Variant into Helical Non-Amyloid Fibrils. *Nat. Commun.* **2022**, *13* (1), 3162. https://doi.org/10.1038/s41467-022-30462-w.

(56) Medeiros-Silva, J.; Jekhmane, S.; Paioni, A. L.; Gawarecka, K.; Baldus, M.; et al. High-Resolution NMR Studies of Antibiotics in Cellular Membranes. *Nat. Commun.* **2018**, *9* (1), 3963. https://doi.org/10.1038/s41467-018-06314-x.

(57) Mani, R.; Cady, S. D.; Tang, M.; Waring, A. J.; Lehrer, R. I.; Hong, M. Membrane-Dependent Oligomeric Structure and Pore Formation of a β-Hairpin Antimicrobial Peptide in Lipid

Bilayers from Solid-State NMR. *Proc. Natl. Acad. Sci.* **2006**, *103* (44), 16242–16247. https://doi.org/10.1073/pnas.0605079103.

(58) Kumar, P.; Kizhakkedathu, J. N.; Straus, S. K. Antimicrobial Peptides: Diversity, Mechanism of Action and Strategies to Improve the Activity and Biocompatibility In Vivo. *Biomolecules* **2018**, *8* (1). https://doi.org/10.3390/BIOM8010004.

(59) Yan, Y.; Li, Y.; Zhang, Z.; Wang, X.; Niu, Y.; et al. Advances of Peptides for Antibacterial Applications. *Colloids Surfaces B Biointerfaces* **2021**, *202*, 111682. https://doi.org/10.1016/j.colsurfb.2021.111682.

(60) Yilmaz, N.; Kobayashi, T. Visualization of Lipid Membrane Reorganization Induced by a Pore-Forming Toxin Using High-Speed Atomic Force Microscopy. *ACS Nano* **2015**, *9* (8), 7960–7967. https://doi.org/10.1021/acsnano.5b01041.

(61) Jiao, F.; Ruan, Y.; Scheuring, S. High-Speed Atomic Force Microscopy to Study Pore-Forming Proteins; 2021; pp 189–217. https://doi.org/10.1016/bs.mie.2021.01.033.

(62) Maimon, T.; Elad, N.; Dahan, I.; Medalia, O. The Human Nuclear Pore Complex as Revealed by Cryo-Electron Tomography. *Structure* **2012**, *20* (6), 998–1006. https://doi.org/10.1016/j.str.2012.03.025.

(63) Sharp, T. H.; Koster, A. J.; Gros, P. Heterogeneous MAC Initiator and Pore Structures in a Lipid Bilayer by Phase-Plate Cryo-Electron Tomography. *Cell Rep.* **2016**, *15* (1), 1–8. https://doi.org/10.1016/j.celrep.2016.03.002.

Supplementary Information

Table S1. Sequences of Plectasin DNA and mutant primers.

Name	Sequence
Plectasin DNA	GGA TTC GGT TGT AAT GGA CCC TGG **GAC** GAG GAT GAC **ATG CAG** TGC CAT AAT CAT TGT AAA TCT ATA AAA GGC TAT AAG GGA GGG TAT TGC GCG AAA GGC GGT TTT GTT TGT AAG TGC TAT
Primers	
D9N FW	TGT AAT GGA CCC TGG **AAC** GAG GAT GAC ATG CAG
D9N RV	CTG CAT GTC ATC CTC **GTT** CCA GGG TCC ATT ACA
D9N M13L FW	TGT AAT GGA CCC TGG **AAC** GAG GAT GAC **CTG** CAG TGC CAT AAT CAT
D9N M13L RV	ATG ATT ATG GCA CTG CAG GTC ATC CTC **GTT** CCA GGG TCC ATT ACA
D9N Q14R FW	TGT AAT GGA CCC TGG **AAC** GAG GAT GAC ATG **CGG** TGC CAT AAT CAT TGT
D9N Q14R RV	ACA ATG ATT ATG GCA **CCG** CAT GTC ATC CTC **GTT** CCA GGG TCC ATT ACA
M13L FW	TGG GAC GAG GAT GAC **CTG** CAG TGC CAT AAT CAT
M13L RV	ATG ATT ATG GCA CTG **CAG** GTC ATC CTC GTC CCA
M13L Q14R FW	TGG GAC GAG GAT GAC **CTG CGG** TGC CAT AAT CAT TGT
M13L Q14R RV	ACA ATG ATT ATG GCA **CCG CAG** GTC ATC CTC GTC CCA
Q14R FW	GAC GAG GAT GAC ATG **CGG** TGC CAT AAT CAT TGT
Q14R RV	ACA ATG ATT ATG GCA **CCG** CAT GTC ATC CTC GTC
Sequencing primer FW	AGG ATC GAG ATC TCG ATC CC
Sequencing primer RV	GGG TTA TGC TAG TTA TTG CTC AGC

Table S2. Solution NMR assignments of plectasin and plectasin mutants

RESIDUE	WILDTYPE PLECTASIN		NZ2114		D9N		M13L		Q14R		D9N M13L		D9N Q14R		M13L Q14R	
	δN (ppm)	δH (ppm)	δN (ppm)	δH (ppm)	δN (ppm)	δH (ppm)	δN (ppm)	δH (ppm)	δN (ppm)	δH (ppm)	δN (ppm)	δH (ppm)	δN (ppm)	δH (ppm)	δN (ppm)	δH (ppm)
G3	100.36	7.949	101.34	8.102	100.789	7.95	100.347	7.932	100.386	8.072	100.675	7.933	101.279	8.1	100.391	8.071
C4	122.579	7.563	121.856	7.657	122.276	7.608	122.556	7.57	122.393	7.593	122.395	7.607	122.105	7.592	122.399	7.603
N5	121.042	8.192	121.074	8.102	121.146	8.054	120.987	8.198	121.046	8.218	121.181	8.051	121.19	8.11	121.034	8.226
N5 SIDE CHAIN	114.908	6.809	114.016	6.984	114.283	6.979	114.925	6.813	114.657	7.501	114.318	6.981	113.994	6.96	114.648	7.517
N5 SIDE CHAIN	114.915	7.441	114.019	7.374	114.33	7.327	114.909	7.45	114.657	6.757	114.385	7.331	114.021	7.358	114.657	6.767
G6	109.376	7.209	109.63	7.425	109.686	7.381	109.351	7.222	109.266	7.216	109.678	7.381	109.637	7.408	109.263	7.234
W8	116.048	7.33	118.066	7.914	117.609	7.88	116.112	7.343	116.357	7.357	117.555	7.89	117.994	7.901	116.285	7.362
W8 SIDE CHAIN	129.86	10.098	129.181	10.066	129.126	10.048	129.867	10.102	129.984	10.105	129.119	10.047	129.161	10.053	129.954	10.111
D/N9	123.167	7.611	121.06	8.003	121.087	7.943	123.187	7.632	123.079	7.616	121.169	7.955	121.1	7.977	123.124	7.648
N9 SIDE CHAIN			113.183	6.947	113.057	6.938					113.027	6.94	113.207	6.937		
N9 SIDE CHAIN			113.206	7.49	113.078	7.467					113.037	7.46	112.969	7.475		
E10	121.374	8.156	121.369	8.419	121.356	8.392	121.447	8.153	121.625	8.179	121.358	8.39	121.379	8.407	121.631	8.179
D11	125.167	8.127	124.097	8.202	124.234	8.211	125.252	8.121	125.048	8.098	124.516	8.197	124.019	8.203	125.274	8.105
D12	123.259	8.397	122.129	8.183	122.751	8.31	123.061	8.342	123.253	8.383	122.548	8.25	122.44	8.23	123.013	8.322
M/L13	117.366	8.181	120.145	8.091	117.777	8.269	119.445	7.968	117.476	8.19	119.798	8.044	118.155	8.315	119.588	7.983
Q/R14	120.817	7.596	120.656	7.583	120.748	7.717	119.79	7.522	121.728	7.622	119.726	7.619	121.825	7.636	120.752	7.543
R14 SIDE CHAIN	111.915	6.897			111.603	6.849	111.959	6.9			111.601	6.857				
R14 SIDE CHAIN	111.922	7.706			111.59	7.7	111.956	7.724			111.607	7.708				
C15	121.223	7.322	120.583	7.648	121.352	7.453	121.012	7.34	121.102	7.364	121.146	7.441	121.535	7.721	121.327	7.39
H16	122.193	9	122.2	8.931	122.079	8.934	122.34	9.028	122.213	9.004	122.351	8.981	121.998	8.908	122.384	9.031
N17	115.024	8.381	114.993	8.575	114.968	8.425	115.099	8.508	114.896	8.403	115.128	8.554	114.969	8.455	115.039	8.537
N17 SIDE CHAIN	111.78	7.464	111.682	7.486	111.759	7.465	111.584	7.465	111.962	6.878	111.537	7.462	111.859	7.479	111.749	6.842

Table S2. Solution NMR assignments of plectasin and plectasin mutants (continued)

RESIDUE	WILDTYPE PLECTASIN		NZ2114		D9N		M13L		Q14R		D9N M13L		D9N Q14R		M13L Q14R	
	δN (ppm)	δH (ppm)	δN (ppm)	δH (ppm)	δN (ppm)	δH (ppm)	δN (ppm)	δH (ppm)	δN (ppm)	δH (ppm)	δN (ppm)	δH (ppm)	δN (ppm)	δH (ppm)	δN (ppm)	δH (ppm)
N17 SIDE CHAIN	111.772	6.849	111.684	6.852	111.787	6.952	111.588	6.807	111.974	7.482	111.588	6.954	111.808	6.889	111.757	7.485
H18	121.641	7.968	122.321	8.019	121.739	7.977	122.106	7.996	121.899	7.958	121.902	8.002	121.965	7.989	122.247	7.999
C19	120.336	8.679	120.11	8.625	120.219	8.629	120.275	8.698	120.246	8.671	120.335	8.651	120.113	8.598	120.287	8.699
K20	114.304	7.788	114.293	7.793	114.327	7.78	114.263	7.808	114.219	7.781	114.326	7.793	114.287	7.767	114.201	7.801
S21	114.393	7.33	114.498	7.392	114.259	7.432	114.576	7.382	114.467	7.358	114.257	7.434	114.38	7.351	114.569	7.391
I22	125.817	7.543	125.895	7.566	125.835	7.545	125.801	7.56	125.851	7.555	125.902	7.547	125.895	7.546	125.877	7.568
K23	126.356	8.097	126.335	8.108	126.354	8.102	126.195	8.083	126.351	8.101	126.37	8.104	126.394	8.106	126.293	8.1
Y25	119.701	7.676	119.741	7.706	119.709	7.686	119.724	7.693	119.68	7.686	119.703	7.686	119.714	7.69	119.717	7.699
K26	120.736	10.604	120.706	10.61	120.721	10.613	120.709	10.595	120.735	10.615	120.739	10.616	120.679	10.616	120.735	10.618
G27	106.82	7.252	106.893	7.289	106.825	7.267	106.857	7.264	106.839	7.263	106.896	7.267	106.832	7.271	106.899	7.272
G28	107.611	8.694	107.582	8.792	107.545	8.708	107.609	8.708	107.627	8.725	107.589	8.738	107.535	8.743	107.637	8.766
Y29	115.441	8.376	115.675	8.448	115.713	8.433	115.421	8.38	115.406	8.369	115.637	8.418	115.807	8.441	115.344	8.373
C30	117.491	9.129	117.788	9.061	117.626	9.078	117.531	9.141	117.526	9.12	117.586	9.085	117.713	9.053	117.521	9.138
A31	129.046	9.583	129.379	9.495	129.216	9.521	129.009	9.594	129.039	9.58	129.164	9.536	129.425	9.49	129.046	9.582
K32	119.087	8.887	119.387	8.913	119.274	8.872	119.001	8.897	119.091	8.897	119.236	8.872	119.484	8.887	119.096	8.909
G33	109.536	8.792	109.137	8.829	109.402	8.816	109.251	8.81	109.589	8.783	109.217	8.809	109.223	8.815	109.46	8.777
G34	104.025	7.387	104.271	7.429	104.128	7.443	104.101	7.381	104.138	7.391	104.149	7.446	104.208	7.431	104.181	7.389
F35	116.334	7.211	116.887	7.334	116.942	7.347	116.281	7.2	116.376	7.216	116.941	7.343	116.934	7.36	116.322	7.214
V36	118.053	7.672	118.47	7.724	118.45	7.701	118.043	7.683	118.07	7.677	118.459	7.702	118.448	7.707	118.112	7.692
C37	127.142	8.741	127.146	8.771	127.231	8.761	127.104	8.734	127.154	8.74	127.274	8.758	127.141	8.767	127.116	8.737
K38	135.977	8.974	135.829	9.006	135.917	9.008	135.969	8.978	135.922	8.98	135.931	9.003	135.83	9.01	135.865	8.983
C39	121.204	7.829	121.132	7.855	121.171	7.847	121.195	7.822	121.21	7.828	121.153	7.837	121.165	7.857	121.203	7.824
Y40	126.279	8.303	126.281	8.328	126.276	8.311	126.286	8.313	126.302	8.31	126.297	8.315	126.269	8.312	126.302	8.325

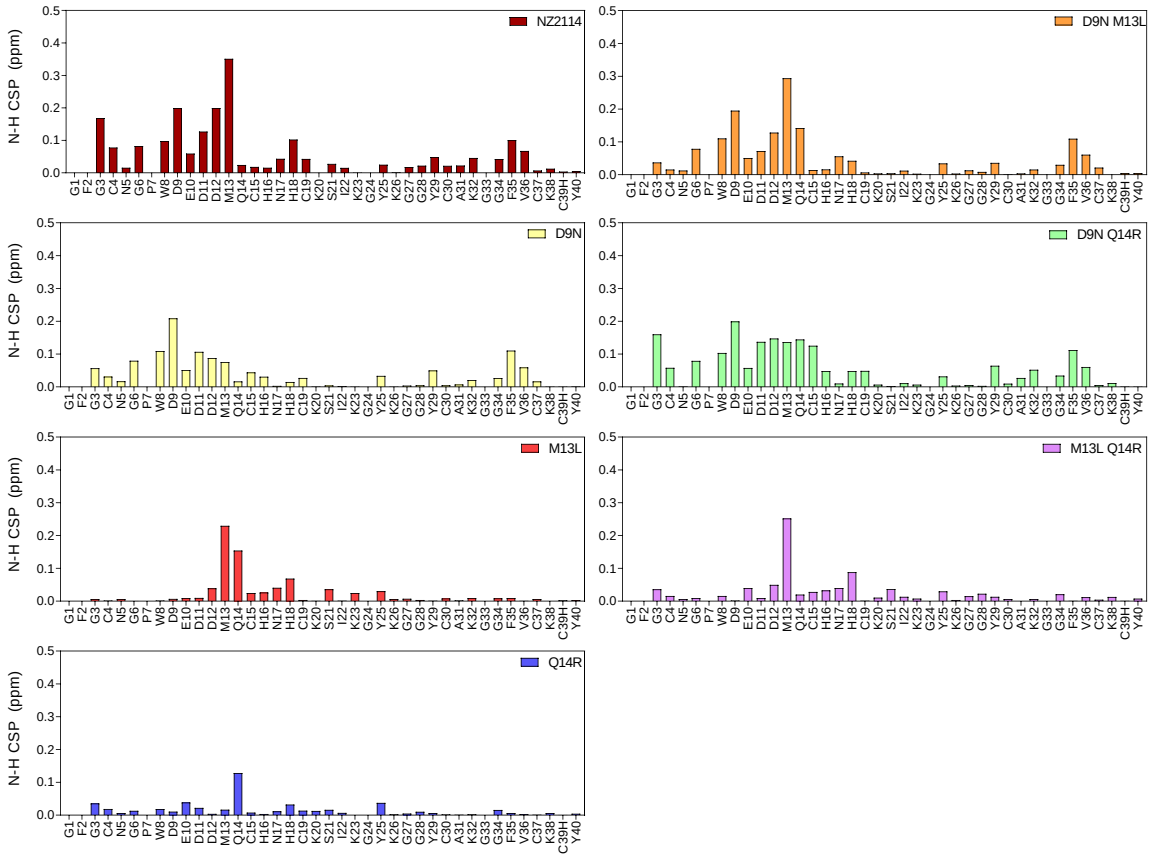

Figure S1. Absolute chemical shift differences (ppm) summed between H_N and N for NZ2114 and the mutant plectasins compared to wildtype plectasin.

Table S3. Inhibition zone diameter (mm) of plectasin and its mutants against MRSA, MSSA and *S. simulans*.

	MRSA				MSSA				*S. simulans*			
	1000 nmol	500 nmol	250 nmol	125 nmol	1000 nmol	500 nmol	250 nmol	125 nmol	1000 nmol	500 nmol	250 nmol	125 nmol
Plectasin	8.8	7.0	4.8	4.5	7.3	6.3	6.1	5.1	13.1	10.8	8.6	6.9
D9N	10.1	9.0	5.8	4.8	8.1	7.3	6.7	6.2	13.3	11.7	10.1	7.6
M13L	8.8	7.2	4.2	4.1	7.9	6.9	6.3	5.7	13.1	10.9	8.7	6.6
Q14R	10.5	8.2	5.7	5.2	8.7	7.9	6.7	6.4	14.8	13.0	11.4	9.3
D9N M13L	10.4	8.6	6.7	5.4	8.6	7.4	6.4	5.6	13.7	12.1	10.5	9.0
D9N Q14R	11.7	10.6	7.9	7.3	9.6	8.8	7.9	7.0	15.2	13.9	12.6	11.0
M13L Q14R	11.3	9.3	7.3	5.8	9.0	8.0	6.9	5.8	14.5	13.3	11.7	9.5
NZ2114	11.6	10.4	8.5	7.2	9.7	8.4	7.7	7.0	14.7	13.1	12.0	10.4

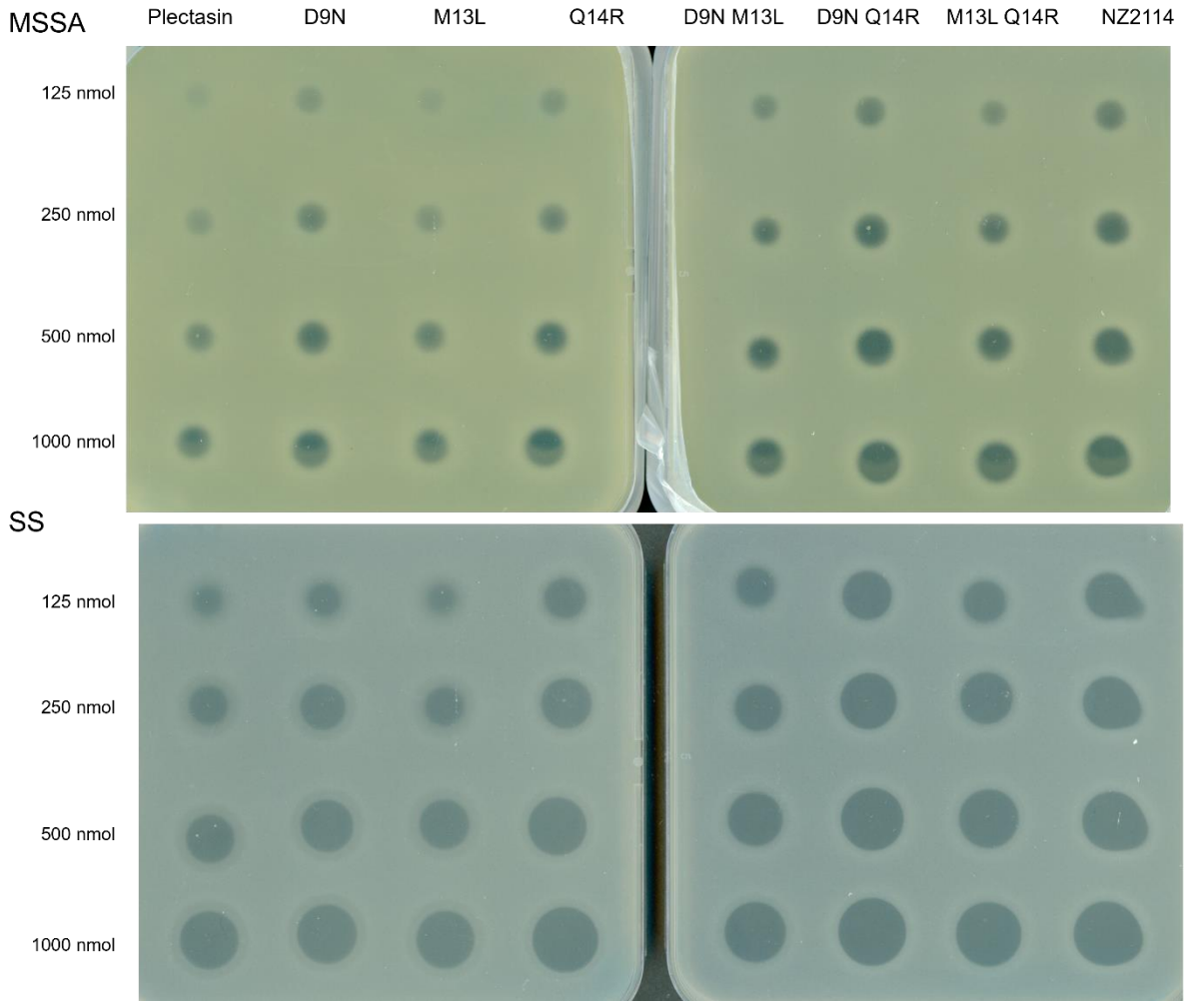

Figure S2. Inhibition zone assay of plectasin and the mutants against methicillin-resistant *S. aureus* (MSSA) and *S. simulans* (SS). The amount of loaded peptide was 125-1000 nmol in ~5 µL PBS.